This is a peer-reviewed, accepted author manuscript of the following conference paper: Fusiek, G., & Niewczas, P. (2022). Design of an optical sensor with varied sensitivities for overhead line sag, temperature and vibration monitoring. In
2022 IEEE International Instrumentation and Measurement Technology Conference (I2MTC) IEEE.

Design of an optical sensor with varied sensitivities for overhead line sag, temperature and vibration monitoring

Grzegorz Fusiek and Pawel Niewczas
Department of Electronic and Electrical Engineering, University of Strathclyde, Glasgow, United Kingdom
g.fusiek@strath.ac.uk

Abstract— This paper reports on the design of a fiber-optic sag, temperature, and vibration sensor to implement overhead line (OHL) dynamic rating and health monitoring in electrical power networks. The proposed sensor is based on the fiber Bragg grating technology for compatibility with a suite of photonic voltage and current sensors previously developed by the authors. A range of different strain transfer and attachment structures for an FBG-based strain sensor that facilitate varied strain transfer from the conductor to the FBG are considered and the expected sensor performance is evaluated through software simulations and the finite element analysis. The results suggest that the proposed sensor, when fabricated, should be a valuable tool for the conductor sag, temperature, and vibration monitoring. The choice of a strain transfer and attachment structure to achieve desired sensitivity can be tailored based on the requirements of a given application.

Keywords— Fiber Bragg grating, optical sag sensor, power system instrumentation, overhead power line health monitoring

I. INTRODUCTION

Conductors are integral components of overhead power lines in electricity transmission and distribution networks. There are different sizes and types of conductors made of either copper or aluminum alloys which can be reinforced with other materials such as steel or composite. Copper conductors can be either soft (annealed) drawn or hard drawn. The main types of aluminum-based conductors include: AAC – All Aluminum Conductor, AAAC – All Aluminum Alloy Conductor, ACSR – Aluminum Conductor Steel Reinforced, ACAR – Aluminum Conductor Alloy Reinforced, ACCC – Aluminum Conductor Composite Core.

Conductors when suspended between two poles are not fully stretched but are hanging with a middle section below the level of supports to which the ends of the conductors are attached. The vertical difference in level between points of support and the lowest point of the conductor is defined as sag of the conductor. Due to its weight, the conductor is constantly in tension and its elongation is influenced by thermal strain, elastic strain, and long-time creep strain. The thermal strain varies with temperature changes in the air, but it is also caused by the rise in temperature due to the current in the conductor. The elastic strain varies with wind and ice loads. The long-time creep strain is a permanent elongation which will only get larger with time, and occurs due to self-weight of the conductor and ice loads [1].

Sag protects the conductor from excessive tension to avoid its damage and ensures that the sufficient clearance between the conductor and the ground is maintained. Therefore, monitoring the level of sag is of great importance, allowing to extend the conductor lifetime and to ensure safety.

High-temperature low-sag (HTLS) conductors replacing original ACSR conductors with approximately the same diameter is one of the techniques to increase current in the energy transmission and thus increasing the transmission capacity of overhead lines. HTLS conductors are capable of withstanding high temperature continuous operation in the range of 200 °C without significant loss of tensile strength or increase in sag [2]. However, as other overhead power lines, they are subject to wind and ice loads which generate vibrations of different frequencies leading to potential damage of the conductors, for example, due to the fretting effect [3]–[5].

The key motivation of the work presented in this paper is to design optical sensors that would allow for the overhead line sag, temperature and vibration monitoring, while remaining compatible with a suite of voltage and current sensors based on the fibre Bragg gratings (FBGs) technology, previously developed by the authors [6]–[8]. The proposed sensors, when combined with the voltage and current sensors, can offer a unified single platform technology for power system dynamic rating and stability control and overhead power line health monitoring, offering early warning data about incipient mechanical failures.

Consequently, this paper concentrates on the design and theoretical evaluation of the optical overhead line sag, temperature and vibration sensor combining a commercially available temperature compensated strain sensor and bespoke mechanical structures to enable installation on a conductor and application-dependent strain transfer to measure the conductor mechanical parameters with sufficient resolution and dynamic range.

II. SAG IN OVERHEAD POWER LINES

A. Sag and tension of the conductor

The conductor sag-tension calculations are typically based on the catenary equation, which describes an entirely flexible

Research presented in this paper was carried out within the YETIS project. YETIS is funded by Energy Catalyst, an Innovate UK programme which is funded by the Foreign, Commonwealth and Development Office (FCDO). All data underpinning this publication are openly available from the University of Strathclyde KnowledgeBase at https://doi.org/10.15129/10404f32-af01-4ccb-9904-810a6ebf1e28

rope rigidly fixed at both ends. The catenary equation is defined using hyperbolic sine or cosine functions. It can also be approximated by a parabolic function. The main difference between a catenary equation and the parabolic approximation is that catenary assumes a constant weight per unit length through the conductor while the parabolic equation assumes an invariable weight per unit horizontal length. This simplification causes the sag calculation with the parabolic approximation to be smaller than when it is estimated with the catenary equation [9].

The shape of a catenary is a function of the conductor weight per unit length weight w, the horizontal component of tension H, span length S, and the maximum sag of the conductor D (see Fig. 1). The catenary equation uses hyperbolic functions while the right hand side of the below equation is an approximation of the hyperbolic cosine using the Maclaurin series expansion [9]:

$$y(x) = \frac{H}{w} cosh\left[\left(\frac{w}{H}x\right) - 1\right] = \frac{wx^2}{2H} \tag{1}$$

For a flat span, the low point is at the center and the wire sag D and can be found by substituting x = S/2.

The sag D calculations can be performed using the following equation [9]:

$$D = \frac{H}{w}\left[cosh\left(\frac{wS}{2H}\right) - 1\right] \cong \frac{wS^2}{8H} \tag{2}$$

The parabolic approximation is sufficiently accurate as long as the sag is below 5% of the span length [10], [11]. The power line sag varies with the conductor temperature, ice, wind loading, and time as the conductor creeps. The horizontal tension H is equal to the conductor tension in the middle of the span shown in Fig. 1. At the endpoints, where the wire is fixed to the insulators, the conductor tension F is equal to the horizontal tension H plus the conductor weight per unit length w multiplied by the sag D, according to the following equation [9], [10]:

$$F = H + wD \tag{3}$$

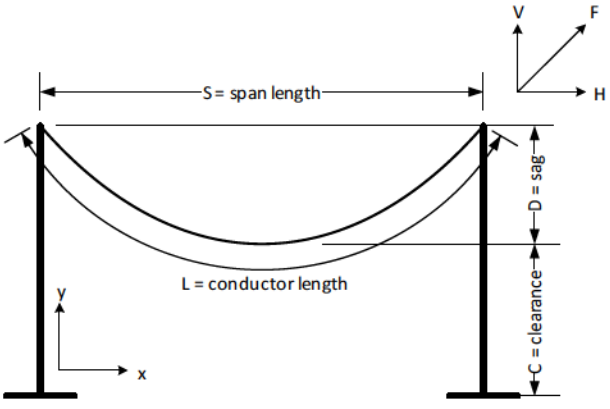

Fig. 1. The catenary curve of the conductor hanging between two poles.

To perform sag-tension calculations only the horizontal tension component H can be used. The conductor length in the span can be calculated with the application of a catenary equation using the following equation [9], [10]:

$$L = \frac{2H}{w}\sinh\left(\frac{Sw}{2H}\right) \tag{4}$$

Equation (5) represents the parabolic approximation of the catenary equation. The hyperbolic sine in (1) can be replaced by a simplified form, and then the length of the wire can be described as presented in (2) [9], [10]:

$$L = S\left(1 + \frac{S^2w^2}{24H^2}\right) \tag{5}$$

However, taking into account sag D, the total length of the conductor L can be expressed according to [9], [10]:

$$L = S + \frac{8D^2}{3S} \tag{6}$$

A simple transformation of (6) allows the determination of the sag D as a function of the distance between the poles S and the actual length of the wire L, which can be expressed by the following equation [9], [10]:

$$D = \sqrt{\frac{3S(L-S)}{8}} \tag{7}$$

where the difference between the conductor length L and span length S is defined as the conductor slack.

The conductor strain measurement can be performed using a strain sensor mounted between two anchoring clamps that are attached to the conductor. Assuming there is no slippage of the clamps on the conductor and the strain transfer from the conductor to the sensor is 100%, the conductor sag D can be calculated as

$$D = \sqrt{\frac{3S(L_c(1+\varepsilon) - S)}{8}} \tag{8}$$

where L_c is the initial conductor length and ε is the strain measured by the sensor equal to the change in the distance between the clamps (a relative elongation of L_c).

It should be noted that (8) is valid for the case where the sensor is installed on the line before it is tensioned. For the case where the sensor is installed after the conductor has already been tensioned (without the sensor), only the difference in strain $\Delta\varepsilon$, and consequently the difference in sag ΔD can be measured. The initial line parameters including the conductor horizontal tension, the sag and the conductor length at the conductor installation are required to calculate the absolute sag and clearance to the ground.

B. Vibration in the conductor

Wind-induced conductor movements are generally caused by aeolian vibrations, conductor galloping, and wake-induced oscillations. Aeolian conductor vibrations are the most commonly reported type that contribute to the long-term damage of the power conductor wires and its fittings [12]. They are low-amplitude high-frequency vortex shedding phenomena characterized by vibration frequencies in the range of 3 – 120 Hz, with amplitudes that can reach the conductor diameter at lower frequencies [13], [14]. For the aeolian vibrations wind speed is in the range of 0.5 to 10 m/s.

Another type of vibration is the conductor galloping which are periodic changes of the mechanical stress with a large vertical amplitude (up to ±1 times the sag) with frequencies of 0.2–1.5 Hz. The phenomenon is often caused by nonsymmetric ice build-up on the conductor and wind [15], [16]. It causes conductor fretting and safety issues.

The OHL sensor will be required to have sufficient sensitivity to detect the vibration on the line, particularly the aeolian vibrations that are of a lower magnitude. Vibration analysis will be possible with suitable signal processing techniques such as FFT analysis.

III. Optical OHL sensor design

A. Sensor operational requirements

The conductor considered in this research is made of hard drawn copper (HDC) with a cross-section area of 70 mm^2 and 10.5 mm diameter. The line span is assumed to be 80 m with both ends of the conductor fixed to the poles at the same level. The conductor weight per unit length and elastic modulus are assumed 5.81 N/m and 104.9 GPa, respectively.

From the equations presented in Section II, the conductor initial length is estimated as 80.02 m and its sag as 0.77 m assuming that the conductor was installed at 15 °C with the initial horizontal tension of 6 kN. equal to 25% of the rated tensile strength (RTS, 24 kN) [17].

It was estimated that the strain generated in the conductor due to wind speed as high as 50 m/s would be approximately 500 με, and a temperature change of +50 °C would generate thermal strain of 850 με in the conductor.

Since the aeolian vibration amplitude could reach the diameter of the conductor, the strain generated in the conductor would be below ±10 με. During galloping, the vertical amplitude of the vibration could be up to ±1 times the sag. The strain generated in the considered conductor at wind speeds up to 50 m/s in the -15÷65 °C temperature range is expected to remain below 1.5 mε. As the commercially available FBG interrogators offer the strain measurement resolution of 1÷2 με, monitoring the aeolian vibrations with amplitudes below 10% of the maximum range would not be possible. To allow for detection of aeolian vibrations with smaller amplitudes, strain amplification would be required. On the other hand, for applications where the measured strain is relatively large reaching several mε, the strain transfer attenuation would be required. Therefore, several different sensor designs were considered to allow for detection of small amplitude aeolian vibrations and large sag and strain measurements.

B. Strain sensor specifications

The proposed optical OHL sensor incorporates a commercially available strain sensor, model T220, fabricated by Technica SA, which contains two FBGs (strain and temperature) packaged in a metal (SS316) enclosure, secured at both ends with strain relief buffers and terminated with 3 mm high temperature armored cables. The sensors can be designed for operating temperatures up to 200 °C and thus be suitable for the HTLS line monitoring applications. Their measurement accuracy as claimed by the supplier is < 0.5 % full-scale (FS) including any hysteresis, nonlinearities, and the repeatability of the sensor. The sensor strain range is ±2000 με with adjustable offset. The device has the ingress protection rating of IP67. Each sensor is surrounded by a 0.2 mm metal sheet (SS304) that is suitable for spot-welding of the sensor to the monitored structure. The sensor strain sensitivity based on the calibration data provided by the manufacturer is approximately 1.2 pm/με.

The strain sensor cannot be directly mounted on the overhead line and requires suitable metallic strain transfer and attachment structures to provide measurements of sag, temperature and vibration on the overhead line conductor. The following sections provide the design of the OHL sensor.

C. Construction of optical sag sensor

A conceptual drawing of the proposed sag sensor installed on a conductor is shown in Fig. 2. The strain sensor (T220) will be spot welded to a 2 mm thick stainless steel mounting plate secured between metal clamps and fastened to the conductor with bolts. An identical second plate is mounted on the opposite side of the conductor to ensure symmetry of strain response, compensating any bending moments that may occur. The distance between the plates and the conductor is approximately 5 mm.

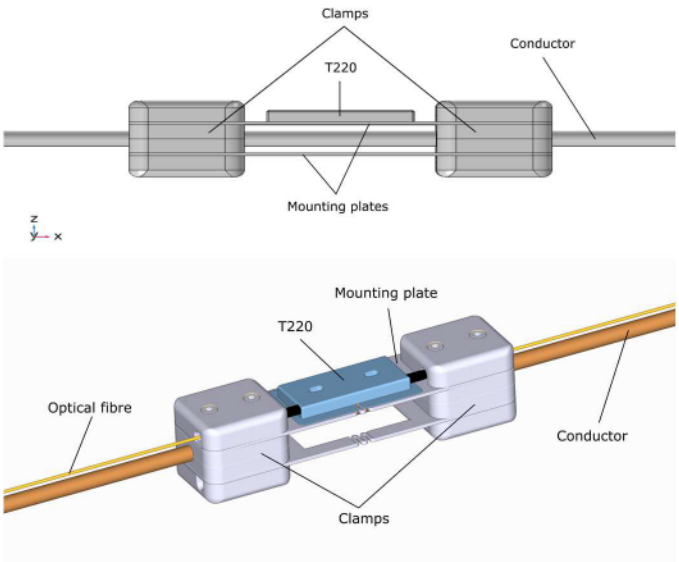

Fig. 2. Optical sag sensor construction.

In the initial design, it is proposed that the T220 mounting plate are made of SS304 as the strain sensor base for welding is made of 0.2 mm SS304 shim. By selecting the sag sensor materials with a similar coefficient of thermal expansion

(CTE), strain and thermal expansion should be matched to that of the conductor. Also, by using materials with a similar galvanic potential, galvanic corrosion should be eliminated. To match the materials with the copper conductor, the use of bronze, brass or SS304 for the clamps is recommended. The anti-corona lacquer or conductive paint can be used to additionally protect the components against the moisture and galvanic corrosion.

It should be noted that the clamps will have to be redesigned for different types of conductors. The design will be dependent on the conductor diameter and material. For example, for HTLS lines or ACCC conductors, aluminum clamps would have to be used for a given diameter of the conductor.

IV. Software Simulations

To verify the expected strain sensor performance and strain transfer between the conductor and the sensor, the proposed mechanical structures' geometries were imported to COMSOL Multiphysics® software and the finite element analysis (FEA) was performed. The below analysis does not take into account the T220 sensor stiffness. The T220 stiffness, however, was assumed much lower than the plates and the conductor and not affecting the results significantly.

A. Stress and strain modeling

In the first study, the sensor was assumed to be attached to a copper conductor and its strain response was analyzed when subjected to an axial load at room temperature. It was assumed that the sensor, the mounting plate, and the clamps were made of SS304. Various plates were considered to adjust the strain transfer from the conductor to the sag sensor structure.

For the mounting plates having greater stiffness than the conductor, strain in the conductor between the clamps is reduced as shown in Fig. 3.

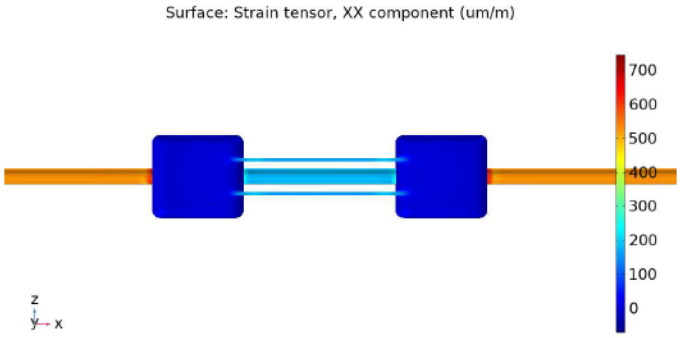

Fig. 3. Strain reduction in the conductor between the clamps due to the sag sensor stiffness.

To minimize this effect, mounting plates with reduced stiffness need to be considered. This can be achieved by changing dimensions of the mounting plates or by reducing the amount of the material by cutting openings in the plates.

Five different mounting plate shapes were proposed as shown in. Fig. 4. For each plate, COMSOL analysis was carried out to find the relationship between the plate displacement and the applied force, and to compare the plates stiffness with the conductor stiffness. The plates axial deformation was simulated when an axial force was applied to one end of the plate while the other end was fixed as shown in Fig. 4. The force was increased from 0 to 1 kN in 100 N steps. Each plate stiffness can be estimated as the ratio of the applied force to the resultant displacement. The simulation results are shown in Fig. 5.

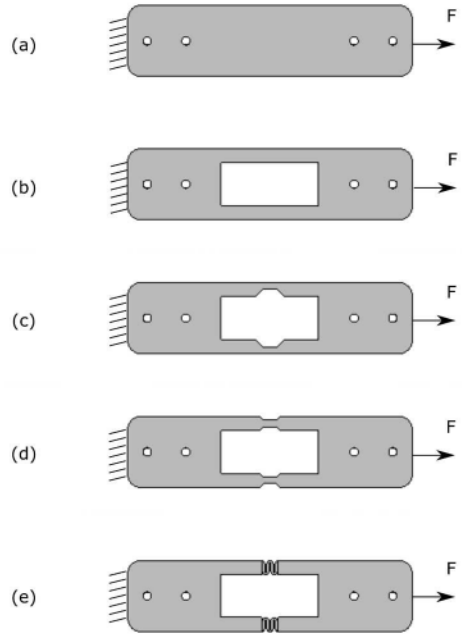

Fig. 4. Mounting plates with different sections removed.

As can be seen from Fig. 5, only the plate with springs (Fig. 4 (e)) has higher compliance (flexibility – the inverse of stiffness) than the conductor. This means that the strain transfer from the conductor to the plate should be high as the plate stiffness will not restrict the conductor elongation between the clamps as in the case of the other plates. The stiffness of the whole assembly will be defined by a combination of the materials, dimensions and shapes of the constituent components of the assembly including the conductor stiffness.

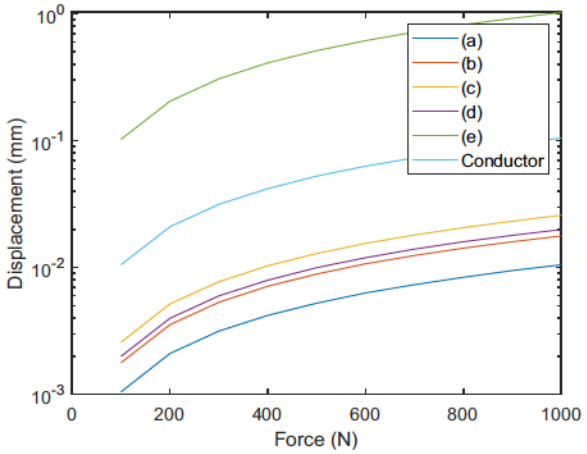

Fig. 5. Displacement vs force for plates (a)-(e) and the conductor. Full scale view to the left and zoomed in view to the right.

To verify strain levels in the conductor between the sensor clamps when different mounting plates are used, FEA was performed in COMSOL. In the simulations, the conductor was fixed at one end and an axial load of 5 kN was applied at the other end of the conductor. The conductor length was 1 m, and the initial distance between the clamps was 100 mm. The example results of the simulations for two constructions ensuring the highest strain transfer are shown in Fig. 6 and Fig. 7.

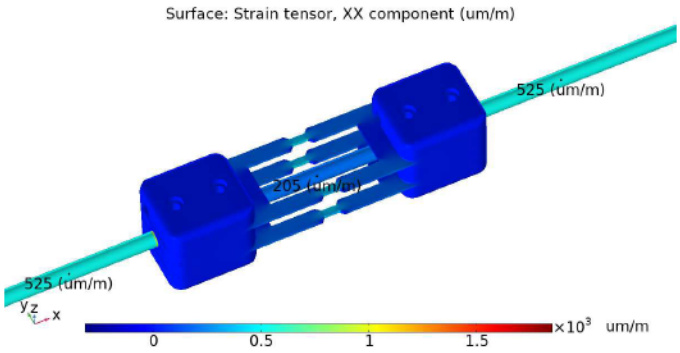

Fig. 6. Strain in the conductor at a load of 5 kN when the sensor mounting plates are as per Fig. 4 (d).

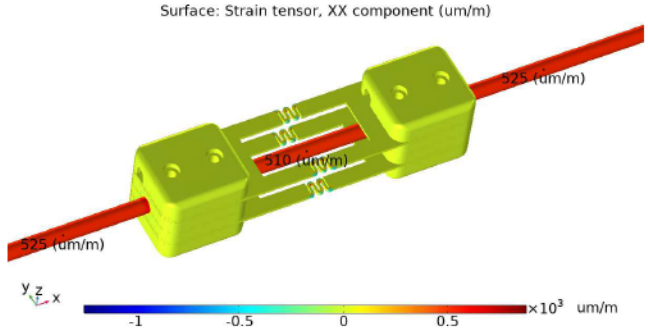

Fig. 7. Strain in the conductor at a load of 5 kN when the sensor mounting plates are as per Fig. 4 (e).

As can be seen from Fig. 6, strain in the conductor section between the clamps is reduced to approximately 40% of the conductor strain outside the clamps for the mounting plates with rectangular openings and with narrowing sections in the middle of the plates. Strain is concentrated in the narrow sections of the plates and reaches nearly 75% of the conductor strain outside the clamps. The simulation results for the sensor with the rectangular holes and springs in the middle of the plates are shown in Fig. 7. The conductor is strained between the clamps to approximately 97% of the conductor strain outside the clamps. In this case, strain is concentrated in the springs, whilest in the remaining regions of the plates there is almost no strain. The strain detected by the sensor can be estimated from the change in the distance between two ends of the spring (13 mm) and the distance between the clamps (100 mm). The strain detected by the sensor when mounted on a plate with springs is nearly 8 times greater than the conductor strain. Therefore, this arrangement will offer strain amplification. Consequently, by adjustments in the design of the mounting plates, strain tranfer from the conductor to the sensor can be tuned depending on the application requirements.

B. Thermal strain modelling

Similar analysis was performed for the assembly when a temperature change of +50 °C was applied to the components. In the study, natural convection at 5 W/m was assumed for all the components in air. As can be seen in Fig. 8, the thermal strain in the conductor between the sensor clamps is almost the same as outside the clamps while the thermal strain in the plates is 93% of the strain in the conductor. The small difference between the thermal strain in the conductor and the plates is due to the slight mismatch between the coefficient of thermal expansion (CTE) of SS304 (17.3×10^{-6} 1/K) and copper (17×10^{-6} 1/K) in the considered temperature range and the software tolerance.

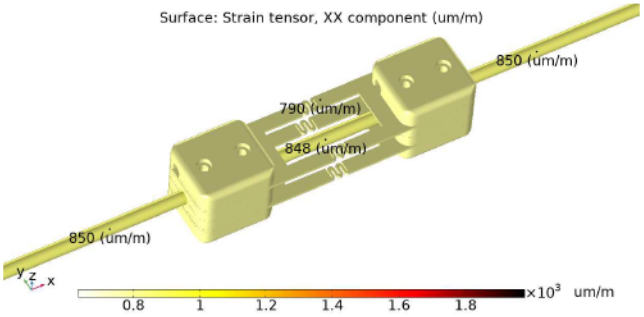

Fig. 8. Thermal strain in the conductor and the sensor plates at + 50° C change in temperature.

A combined effect of thermal and mechanical strain on the assembly at 5 kN load applied to the conductor is shown in Fig. 9. Strain in the conductor between the sensor clamps is 99% of that outside the clamps while strain in the plates increased by less than 2% in comparison to the case of the unloaded conductor. The small differences in the results are due to the FEA limitations and the tolerance on the assumed material specifications.

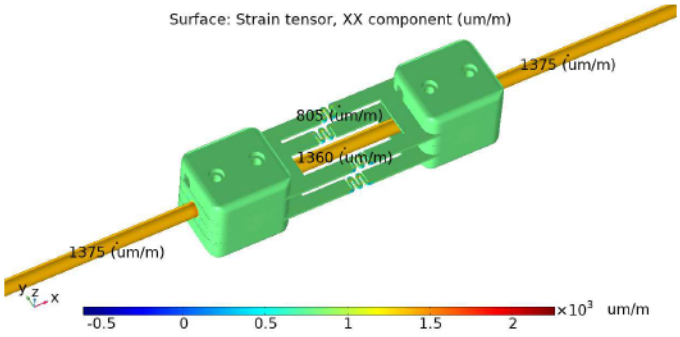

Fig. 9. Thermal and mechanical strain in the conductor and the sensor plates at +50° C change in temperature and a load of 5 kN applied to the conductor.

It should be noted that in the real application the thermal strain in the conductor will increase with the temperature rise

while the tension in the conductor, and hence the mechanical strain, will decrease. Also, the CTEs and other parameters of the materials will be temperature dependent and may have slightly different values from the used in the FEA model depending on the chemical composition of the materials.

The results of the simulation demonstrate that the proposed sensor design will meet the specifications for sag and aeolian vibration monitoring by the sensor, as stated in Section III A. The conductor strain that can be detected by the sensor can range from around 0.2 με to several mε. Depending on the application requirements, strain tranfer from the conductor to the sensor can be adjusted by modifications in the design of the strain sensor mounting plates. The results of the simulations will be verified experimentally in the future.

V. Conclusions

In this paper, the design of an optical sag sensor for overhead line health monitoring in electrical power networks has been presented. The sensor attachment structures ensuring adequate strain transfer from the conductor to the sensor have been discussed and the expected sensor performance was theoretically evaluated through software simulations and the finite element analysis. The theoretical evaluation of the expected sag sensor performance was carried out in COMSOL software. Based on the simulations it was concluded that the OHL sensor when fabricated, should be a valuable tool for the conductor sag, temperature, and vibration monitoring at various environmental conditions.

Future work will focus on the construction of the proposed sensors and their performance validation.

References

[1] L. Sjöholm, "Computational handbook for power line engineers," Stockholm, Sweden, 2017.

[2] B. Subba Reddy and D. Chatterjee, "Performance evaluation of high temperature high current conductors," *IEEE Trans. Dielectr. Electr. Insul.*, vol. 23, no. 3, pp. 1570–1579, 2016, doi: 10.1109/TDEI.2016.005529.

[3] M. Boniardi, S. Cincera, F. D'Errico, and C. Tagliabue, "Fretting Fatigue Phenomena on an all Aluminium Alloy Conductor," in *Key Engineering Materials*, vol. 348–349, 2007, pp. 5–8.

[4] D. Wenzheng, M. Baozhu, X. Zheng, C. Dazhi, and W. Peng, "Finite element analysis on the wire breaking rule of 1×7IWS steel wire rope," *MATEC Web Conf.*, vol. 108, pp. 7–11, 2017, doi: 10.1051/matecconf/201710801002.

[5] CIGRE TF.WG.B2.12.3, *Technical Brochure 324: Sag-tension calculation methods for overhead lines*, no. June. 2007.

[6] J. Nelson *et al.*, "Development and testing of optically-interrogated current sensors," in *2016 IEEE International Workshop on Applied Measurements for Power Systems (AMPS)*, 2016, pp. 1–5, doi: 10.1109/AMPS.2016.7602871.

[7] G. Fusiek, J. Nelson, P. Niewczas, J. Havunen, E. P. Suomalainen, and J. Hallstrom, "Optical voltage sensor for MV networks," *Proc. IEEE Sensors*, vol. 2017-Decem, pp. 1–3, 2017, doi: 10.1109/ICSENS.2017.8234104.

[8] G. Fusiek, P. Niewczas, N. Gordon, P. Orr, and P. Clarkson, "132 kV optical voltage sensor for wide area monitoring, protection and control applications," in *I2MTC 2020 - 2020 IEEE International Instrumentation and Measurement Technology Conference, Proceedings*, 2020.

[9] P. Ramachandran, V. Vittal, and G. T. Heydt, "Mechanical State Estimation for Overhead Transmission Lines With Level Spans," *IEEE Trans. Power Syst.*, vol. 23, no. 3, pp. 908–915, Aug. 2008, doi: 10.1109/TPWRS.2008.926093.

[10] M. Wydra, P. Kisala, D. Harasim, and P. Kacejko, "Overhead transmission line sag estimation using a simple optomechanical system with chirped fiber bragg gratings. part 1: Preliminary measurements," *Sensors (Switzerland)*, vol. 18, no. 1, pp. 1–14, 2018, doi: 10.3390/s18010309.

[11] J. R. Fanchi, "Electric Power Generation and Distribution," in *Energy Technology and Directions for the Future*, Elsevier, 2004, pp. 28–58.

[12] M. A. Alaqil and K. Kopsidas, "Modelling the Structural Dynamics of Electrical Overhead Line Power Conductors."

[13] B. Godard, S. Guerard, and J.-L. Lilien, "Original Real-Time Observations of Aeolian Vibrations on Power-Line Conductors," *IEEE Trans. Power Deliv.*, vol. 26, no. 4, pp. 2111–2117, Oct. 2011, doi: 10.1109/TPWRD.2011.2158859.

[14] L. Bjerkan, "Application of fiber-optic Bragg grating sensors in monitoring environmental loads of overhead power transmission lines," *Appl. Opt.*, vol. 39, no. 4, p. 554, Feb. 2000, doi: 10.1364/AO.39.000554.

[15] Products Preformed Line, "Conductor Galloping Basics," vol. EN-ML-1166, no. February, 2016.

[16] A. S. Richardson, "A study of galloping conductors on a 230 kV transmission line," *Electr. Power Syst. Res.*, vol. 21, no. 1, pp. 43–55, Apr. 1991, doi: 10.1016/0378-7796(91)90036-M.

[17] U. Cosmai, P. Van Dyke, L. Mazzola, and J.-L. Lillien, "Conductor Motions," in *CIGRE brochure 756*, vol. 01, no. June, K. O. Papailiou, Ed. Cham: Springer International Publishing, 2017, pp. 559–711.